RUBIKS - Reconstruction of Undercrust Behaviour with Interconnected (K)cubesatellites

Antonius Adler, David Apellaniz, Christina Bornberg, Colin Dandumont, Océane Dhuicque, Marthe Faber, Sotirios Kechagias, Serena Lisi, Viktor Lundstedt, Martynas Milasevicius, Ana Pagu, Florian Vidal, Lucas Schreiter, Jacob Smith, Sindre Steinsvik

July 24, 2019

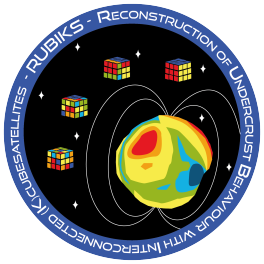

Abstract

RUBIKS (Reconstruction of Undercrust Behaviour with Interconnected (K)cubesatellites) is a nanosatellite mission proposal dedicated to analysing the Earth's mantle. With 8 CubeSats (6U) on two Cartwheel-helix orbits, we propose taking magnetic and gravity measurements of the Earth's interior, in order to gain information on the electrical conductivity and density of the mantle, especially the lower mantle. This mission leads to a better understanding of the composition by allowing for a 3D coupled inversion process and of the dynamics of the mantle through resolving for changes with a high temporal resolution - particularly in view of mantle plume origin and evolution with relation to plate tectonics. In order to achieve this, the payload is two magnetometers on a deployable boom (1 m length) and a GNSS receiver on each satellite. The lifetime mission is 3 years for a total cost estimation of 10 M€.

1 Mission Objectives

In this mission, we aim to answer several outstanding questions in geophysics:

- O1. How can we explain heterogeneities (composition e.g. mineralogy, water content, temperature) in the mantle through electrical conductivity and density anomalies?
- O2. Where do mantle plumes originate and how do they travel through the mantle? What role do the aforementioned heterogeneities play in this process?
- O3. What is the role of mantle plume flow in plate tectonics?
- O4. Is there a link between magnetic and gravity anomalies in the lower mantle?

2 Scientific Background

The Earth is primarily composed of four layers: a solid silicate crust, a solid silicate mantle, a liquid iron outer core, and a solid iron inner core.

Despite representing almost half of the radius of the Earth and most of the volume, the mantle is still insufficiently understood. It is composed of distinct layers, defined by mineral transitions. Broadly, it can be divided into three layers: the upper mantle (100 km - 410 km), the transition zone (410 km - 660 km), and the lower mantle (660 km - 2891 km).

There is significant evidence that the entire mantle is convecting, which implies that it is well mixed ([van Keken et al., 2002]). However, petrological evidence from some lavas suggests that there are reservoirs of a different composition in the mantle ([Harrison et al., 2017]). Therefore, one of the major outstanding questions in Earth Sciences is where these reservoirs are, and why were they not mixed with the rest of the mantle?

2.1 Mantle plumes

Mantle plumes are a mechanism of mantle convection, in which hot material rises through the mantle. When mantle plumes reach the Earth's crust, they result in a type of volcanism known as hotspot volcanism. Beyond this, mantle plumes are not generally understood. Subtle variations in their trace and isotope compositions suggest that they do not originate in the main body of the mantle ([Harrison et al., 2017]). It is still unclear

where they originate (at the core-mantle boundary or in the mantle transition zone), how they interact with the mantle flow and how/if they influence plate tectonics ([Gassmöller et al., 2016]).

2.2 Statement of problem

This section outlines the primary reasons the scientific community has an insufficient understanding of the Earth's mantle.

2.2.1 Scarcity of mantle samples and unreliability of seismic data

A window into the mantle is given by rock samples. Several processes are known to bring samples of the mantle to the surface of the Earth, the main one of which is volcanism. Unfortunately, these samples are limited to the upper mantle and not very much is known about the lower mantle from direct sampling (although high-pressure laboratory experiments of mantle minerals have successfully produced lower mantle minerals before; e.g. [Murakami, 2004]).

Currently, the main tool we have for imaging the mantle is seismology. Seismic waves travel through the mantle and get reflected and refracted based on what material they encounter. When they reach a seismic station, an inversion can be performed in order to learn about the composition of the mantle on the path of the wave. This technique is known as seismic tomography. Due to the scarcity of seismic stations (on land only) the resolution of seismic tomography decreases significantly with depth ([Rawlinson et al., 2014]). In the lower mantle, tomographic models differ significantly both in terms of the shape of the features present, and the magnitude of the signal. Furthermore, the direct detection of plumes is now at the edge of seismic resolution ([Sleep, 2006]).

Seismic velocity profiles can only be used as an indirect means of inferring the internal state and composition of the Earth. Much information can be gained by the integration of widely different data sets, where usually only one set of parameters that a priori do not have anything in common is inverted. For instance, inversion of seismic data gives information on seismic-wave velocities, and electromagnetic sounding data provide knowledge on the electrical conductivity profile, while gravity data tell us about the subsurface density structure ([Khan et al., 2007]). A 3D joint inversion of electromagnetic sounding data, gravity data and seismic velocities with constraints of petrological data (laboratory measurements or physical laws) considerably improve the knowledge about the investigated subsurface ([Khan et al., 2007]) by leading to better compositional and temperature models.

2.2.2 Difficulties in capturing long magnetic field periods

Even though electromagnetic sounding allows to directly probe the Earth, it also has its limitations that have not yet been solved by missions such as CHAMP or SWARM: long electromagnetic sounding periods allow for larger penetration depths in the Earth than short ones. Longer periods ($>$ 3 days) would thus be necessary to image the lower mantle (depth $>$ 440 km). However, the usability of observatory magnetic data for the recovery of global 3-D mantle conductivity structure is limited to the assumption that the source of the variations is well approximated by a large-scale symmetric (magnetospheric) ring current ([Püthe et al., 2015]), described by a single spherical harmonic. However, there has long been evidence for a more complex structure and asymmetry of the magnetospheric ring current. Due to this inaccurate description of the source ([Püthe et al., 2015]), 3D conductivity structures observed in various thermo-chemical models strongly differ both in amplitude and distribution, and are limited to depths of 1600 km for sounding periods of 180 days. This variability in models could be constrained with actual measurements of long-period variations of the magnetic field. The results of [Deschamps and Khan, 2016] show that long-period variations of the magnetic field ($>$ 1 year or longer) may provide key insights on the nature and structure of the deep mantle beyond 1600 km.

2.3 Scientific objectives

2.3.1 Mantle composition (O1)

In the lowermost mantle (2400–2891 km), the seismic structure is dominated by two Large Low Shear-wave Velocity Provinces (LLSVPs) beneath the Pacific and Africa, where shear-wave velocity drops by a few percents compared to its horizontally averaged value ([Deschamps and Khan, 2016])(Figure 1). Together, they cover approximately a quarter of the CMB. The exact nature of LLSVPs is still unclear, but several hints suggest that they result from both thermal and chemical anomalies ([Deschamps and Khan, 2016]). The interpretation of the drop in shear-wave velocity is very ambiguous: there is an ongoing discussion on whether the LLSVPs have a lower- or higher-than-average density ([Trampert, 2004] [Koelemeijer et al., 2016]). Gravity soundings of the deep mantle could shed light on the density structure of seismic structures.

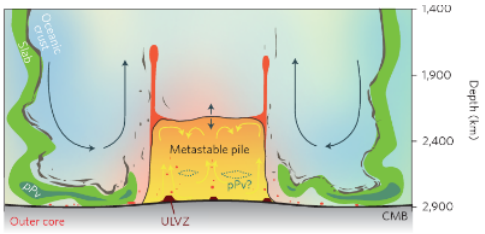

Figure 1: A simplified representation of an LLSVP, showing mantle plumes originating from their edges (after [Garnero et al., 2016])

2.3.2 Origin of plumes (O2)

As mentioned previously, the origin of mantle plumes is not well constrained. Models include: origin on the CMB as purely thermal anomalies ([Dutta and Mandal, 2017]), at the edges of LLSVPs as thermal or thermochemical anomalies ([Harrison et al., 2017]), and at the transition zone ([Miao et al., 2019]). Currently, we are unable to image mantle plumes due to the low resolution of seismic tomography. Since the origin of the plumes directly relates to their composition and influences mantle dynamics, being able to image plumes and trace them to their origin would be significantly advancing the field of geodynamics.

2.3.3 Relationship to tectonics (O3)

Some present-day hotspot locations are found to coincide with plate rifting phenomena, for example, the Afar plume causing the break-up of the Arabian, Nubian and Somalian plates ([Koptev et al., 2018]). An interaction between plumes and nearby diverging plate boundaries, where the flow is deflected from the hotspot to the crustal segment was already suggested in the 1980s ([Koptev et al., 2018]). These observations raise the question of how and under what conditions plume material can flow towards a ridge, and what shape this flow will take. Classical theories ([Dewey and Burke, 1973]) suggest that plume impingement on a non-pre-stressed lithosphere alone can produce plate break-up. However, more recent studies ([Koptev et al., 2018]) suggest that more factors, such as the stress field at the break-up location play a major role in the initiation and evolution of tectonic plate break-up. The role of the plume in this global process still needs to quantified.

Global and local mantle flow information is crucial for the reliability of models attempting to reconstruct or predict plate tectonic evolution. However, mantle flow is often assumed to be constant over large time scales. Dynamic monitoring of flow velocities in the upper mantle could help to improve the already existing geodynamic model of mantle-lithosphere interaction and explain to what extent mantle plumes are driving continental break-up. Additionally, conductivity measurements with a high temporal sampling rate can give insight into the thermal (melt) evolution of the plume on the mantle-lithosphere boundary.

2.3.4 Coupling between gravity and magnetism (O4)

ESA's 4D Earth study suggests that the dynamic topography (several km in height) of the CMB is tightly linked to the mantle and core flow, as well as the densities and viscosity of lower mantle structures (subducted slabs and LLSVPs). The study of [Mandea et al., 2012] suggests that the signature of the core contribution to the gravity field is consistent with the signature of the geomagnetic field. Further coupled gravity and magnetic field observations could provide insight into the monthly and yearly changes that are occurring deep within the Earth.

Heat flux from the core at the core-mantle boundary influences lower mantle dynamics (subducted slabs and LLSVPs). Therefore, the correlation between gravity and magnetic field changes (for example, as observed between the Indian and Atlantic oceans) might be affected by both temporal variations in the core and the dynamics of the lower mantle ([Mandea et al., 2012]). Given that the region of correlation between gravity and magnetism coincides with the South Atlantic Anomaly, the long-standing question of the origin of this anomaly could be resolved.

2.4 State of the Art

2.4.1 Previous magnetic field missions

To derive the electrical conductivity, careful separation of internal and external magnetic sources has to be performed, so highly accurate magnetic measurements at different altitudes are vital. The single Satellite missions Ørsted (1999-2014 at 650 km to 860 km altitude) and Challenging Minisatellite Payload (CHAMP, 2000-2015, below 450 km) provided high accuracy magnetic field Vector measurements. However, given that they only provided single satellite measurements, ionospheric currents could not be estimated.

The Swarm Mission (2013-, 470 km (A/C) and 520 km (B)) is able to resolve ionospheric currents, but only seasonal mean models for the solar quiet can be derived because the lower pair is drifting slowly in local time. Swarm takes about 4 years to cover all local times in all seasons (summer, equinoxes, winter) equally. As the Solar Quiet is depending on the F10.7 index, the temporal variation in the Solar Quiet takes place in significantly smaller timescales. The mission objective of RUBIKS is therefore to capture the solar quiet variations with a time resolution of only a few hours.

2.4.2 Previous gravity missions

The Gravity Recovery And Climate Experiment (GRACE, 2002-2017, 450 to 500 km) was a dedicated gravity mission consisting of two satellites using inter-satellite K-Band ranging. Since 2018 GRACE-FollowOn, having a similar measurement principle is in orbit. Monthly gravity field solutions could be resolved up to degree and order 120. However, the GRACE(-FO) measurements only have a high accuracy in the along-track direction. This may be seen in the longitudinal error showing a strong wave pattern. Furthermore, diurnal temporal resolution is required for the deep mantle (ESA).

The Gravity field and steady-state Ocean Circulation Explorer (GOCE, 2009-2013, 250 km) Mission was able to measure the full gravity gradient tensor, but due to the short baseline of 50 cm the low degree spherical harmonics coefficients could not be estimated with sufficient accuracy. In several models, the GRACE coefficients are used for the low degrees. From degree 70, the models were extended using the static GOCE solution.

RUBIKS is combining the long baseline form of GRACE with the gradiometer measurement principle of GOCE. For that purpose, we use Nanosatellites as proof masses flying in a 3-dimensional formation with a relative distance of 100 km. Two such formations will ensure we are able to solve for diurnal low order degree gravity fields, as required to obtain deep mantle densities.

2.5 Scientific requirements

SR0 Conductivity and density sampling at same points in time and space for the lower mantle d=1000-2900 km

SR1 Measure temporal magnetic field variations – 3D EM sounding for d=100-2900 km

SR1.1: Clearly separate between external and internal field components components

SR1.1.1: Measure primary B-fields produced by external currents

SR1.1.2: High temporal resolution to separate different source signals with overlapping period ranges to all spherical harmonics modelling

SR1.2: Sensitivity to induced B-field at orbit altitude: reliable conductivity and fluid velocity data

SR1.2.1: Improving dynamic core field data (secular variations)

SR1.2.2: Separate induction response in mantle contribution and ocean current

SR2 Measure temporal gravity field variations – 3D density anomalies in lower mantle

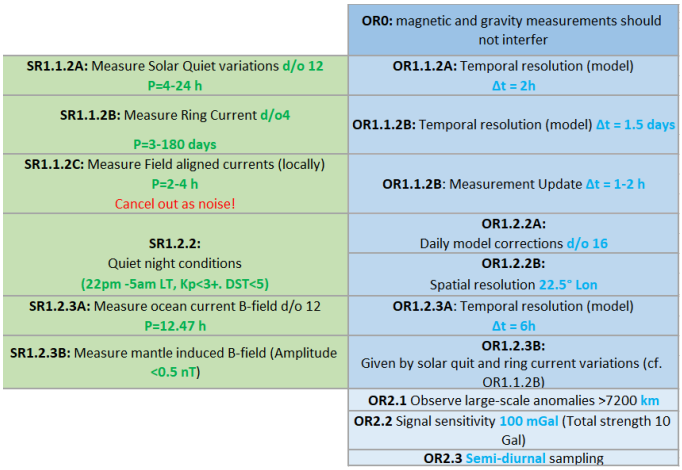

Figure 2: Scientific requirements linking to observational requirements.

To separate internal and external fields, the comprehensive inversion technique is used ([Sabaka and Olsen, 2006]).

The major challenge comes from the curl-free assumption being violated in ionospheric regions above 80 km. Therefore, careful modeling of the ionospheric sources needs to be performed. Furthermore, major geomagnetic field components need to be estimated. The magnetic signal amplitude expected from the induced current is on the 0.5 nT level for 400 km above the crust. As such, it is necessary to capture the signal with an accuracy of roughly 0.2 nT (SR 1.2.3B) to perform proper frequency analysis. The periods which have to be resolved are between 2h and more than 180 days, to allow us to estimate the conductivity from 100 km to more than 1600 km depth. Assuming a dipole-like field, the signal strength is dropping with $1/r^2$. Signal strengths of an induced current at -100 km for different altitudes:

altitude	300 km	400 km	500 km	600 km	1000 km
strength	0.8 nT	0.5 nT	0.35 nT	0.25 nT	0.1 nT

Table 1: Signal strengths of induced current with source at -100 km at different satellite altitudes

2.5.1 Magnetic field requirements (SR1.2)

We need to separate internal and external sources. All these sources have different strengths and need to be modeled with specific temporal resolutions. Referring to [Sabaka and Olsen, 2006] and Kuvshinov (Presentation 4D deep earth, "EM sounding of deep Earth from space and ground"), the external fields, magnetic Ring Current (RC), Field Aligned Currents (FAC) and the Solar-Quiet variation (SQ) need to be observed. Since the Ring Current and the Solar Quiet variation are our major sources for mantle induction, we need the temporal resolution of our models to be below half the periods required for electromagnetic sounding. For the Solar Quiet, these periods are between 4h and 24h, and for the Ring Current, they are between 3 days and 180 days (Kuvshinov et al.). The required spatial resolutions of the models is taken from ([Sabaka and Olsen, 2006]) and compared to the resolution of state-of-the-art models.

The core field (SR 1.2.1) is by far the strongest signal measurable at satellite altitude. It reaches up to 50.000 nT ions and 20.000 nT in equatorial regions. A state of the art model is the CHAOS-6 model, resolved up to spherical harmonic degree 20 and a temporal resolution of 1.2 months (CHAOS-6 Model). Due to spherical harmonic dampening with $(Re/(Re + 400km))^{n-1}$, no coefficient above degree and order 16 have to be estimated. This is because for order 16 at 400 km, the dampening coefficient is 0.42 and no field contribution above degree 16 exceeds 0.31 nT which leads to a contribution of less than 0.15 nT.

However, the core field also has small scale secular variation which needs to be resolved. Therefore, we aim to estimate the secular variation with 1-day resolution, since the smallest periods in the Ring Current for deep EM sounding are 1.5 days. For satellite-based estimation of the core field, the satellite needs to be between 22:00 LT and 5:00 LT, to avoid ionospheric currents on the sun side and to avoid irregularities which are most prominent near dusk and dawn. Furthermore, the magnetic field needs to have quiet conditions ($Kp < 3+$ and $|DST| < 5$). Orbits with nighttime arcs are therefore required (SR1.2.2).

The Ring Current (SR1.1.2B) is the largest external magnetospheric source. It is a large scale current aligned with the geomagnetic dipole equator with a diameter of 2-6 Earth radii, depending on Solar condition. It provides the long period source for EM sounding with periods from 3 d to 180 d, maybe even longer, which allows deeper penetration in the Earth. Due to the small period of 3 d, the ring current needs to be estimated every 1.5 d. To get to 180 d+ frequencies we require a mission lifetime of 3 years. Since the ring current is large scale, it is sufficient to use spherical harmonics up to degree and order 4.

The signal strength is below 5 nT for quiet times. For storms, up to 600 nT have been observed. Even if the EM signal is strong during storms, ionospheric currents and disturbances need to be observed carefully. The full gradient tensor will be used for this purpose. This requires a tetrahedral orbit configuration with a distance of 100 km to 200 km since the major part of the current system is expected to extend from 100 to 400 km on the day-side and the conductivity on the night-side is related to the F Layer and can be expected to be between 300 km and 400 km.

Field aligned currents (SR1.1.2C) are present in the polar regions (65° mag. Lat −75° mag. Lat). Since they show small scale structures, they need to be observed with a high spatial resolution (10 km which implies a magnetic data sampling of 1 Hz) to estimate their strength.

Due to the Solar quiet as EM sounding source, we need to observe the field-aligned currents every 1 to 2 hours. They may reach several hundred nT.

Solar quiet (SR1.1.2A) is a large scale current system on the day-side with a strength of +/- 30 nT. It provides periods for EM sounding from 4 h to 24 h. A state of the art model (difi-3 model) resolves the current system with a full degree and order 12. Since it is not current-free, a Gaussian field separation is not possible. Since a current generates a magnetic ring field, we need access to the rotation of the B field. This requires the full gradient tensor. Since the Tensor provides 4 times more information unidirectionally, we are able to resolve the Ring Current with two passes on the day-side with degree and order 16. We need to update our Solar-Quiet model every 2h, due to the smallest period of 4h.

Ocean currents(SR1.2.3A) are a minor source with a strength of 2 nT at satellite altitude (Irrgang, 2019). They are earth fixed. Since the ocean tides have a well defined period of 12.47 h they need to be modeled with 6h temporal resolution up to degree and order 12 with a model update rate of 6 h.

2.6 Gravity requirements

We want to resolve the deep mantle gravity signal. For this purpose, we refer to a study of Bart Root (TU Delft, 4D Deep Earth). He had shown with simulations, that for deep mantle gravity a model resolution of degree and order 5 is sufficient. This translates to 72° Lon. Since the signal of the geoid height is in the range of 100 m, this can be achieved using GPS only gravity field estimation, even without an accelerometer. In the case of Swarm, the monthly GPS only gravity fields could be computed by absorbing the non-gravitational accelerations using 6 min piecewise constant accelerations ([Jäggi et al., 2016]). The resulting gravity fields have cm accuracy in geoid height. Therefore we use the same approach, but we need to have a 12h temporal resolution in the model to account for the solid earth tides. In addition, make use of a virtual gradiometer with our satellites as proof masses and monitor the relative distance using GNSS double baseline differencing. By this, we can obtain the full gravity gradient tensor and even increase the accuracy of the relative positioning to mm level.

3 Payload

The science requirements on the payload lead to a highly accurate vector magnetometer with 0.2 nT sensitivity and a sampling of 1 Hz. Due to a core field of 50.000 nT we need an attitude knowledge of 1 arcsec to ensure the error in the vector component stays below 0.2 nT. A Position error of 10 m is acceptable for the magnetic field (IGRF-12 Simulation). Also required is a high accuracy (1-3 cm) dual-frequency GNSS receiver with a 0.1 Hz sampling ([Jäggi et al., 2011]).

In order to fulfill the scientific requirements and to make measurements of the magnetic field in three dimensions, the following instruments have been chosen:

- Scalar magnetometer, Coupled Dark State Magnetometer (CDSM)
- Vector magnetometer, Fluxgate magnetometer (FGM).

The CSDM is used to re-calibrate the FGM. For accurate attitude knowledge, two star trackers are placed beside the FGM. All instruments will be placed on a boom to provide magnetic cleanliness. For gravitational measurements a GNSS receiver is implemented: Fast, Orbital, TEC, Observables and Navigation (FOTON).

3.1 FGM

The Fluxgate Magnetometer was launched on the ELFIN mission, in September 2018. The ELFIN mission lifetime is expected to be two years. Given that our mission lifetime is for three years, it is required to test and determine that the instrument will survive our mission duration. The scientific requirements are listed in the table below.

Dynamic range	±50000 nT
Accuracy	< 0.2 nT

Table 2: Scientific requirements

The performances of the FGM are listed in the table below.

Dynamic range	±55000 nT
Resolution	6.5 pT
Noise resolution	0.2 nT/$\sqrt{Hz}$ @ 1 Hz
Relative stability	0.5 nT/h

Table 3: Instrument performances

In Table 3 above it can be observed that, looking at the relative stability of the instrument and at the required accuracy(<0.2nT), it will be necessary to re-calibrate every 20 minutes. The instrument parameters are listed in the table below.

	PCB	**SH**
Power	<1 W	<1 W
Voltage	8 V	8 V
Size	90 mm×90 mm×2 5mm	48 mm×4 8mm×25 mm
Mass	100 g	106 g (1 m cable)

Table 4: Instrument parameters

3.2 CDSM

The Coupled Dark State Magnetometer was launched on the China Seismo-Electromagnetic Satellite (CSES) in February 2018. Due to the 5 year lifetime of the CSES mission, it is expected that the instrument lifetime will be acceptable for the length of our mission. The inputs for this instrument (scientific requirements) are listed in the table below.

Absolute error	< 0.2 nT
Calibration error	< 0.03 nT

Table 5: Scientific requirements

The performances of this instrument are listed in the table below.

Range	20000 nT 100000 nT
Noise	<30 pT/$\sqrt{Hz}$ @ 1 Hz

Table 6: Performances

The parameters of the instrument are listed in the table below.

	PCB	**SH**	**Harness**
Power	2.836 W	0.72 W	
Mass	1033 g	340 g	299 g
Size	20 mm×100 mm×10 0mm	50 mm×10 mm×10 mm	

Table 7: Parameters of the instrument

3.3 Star trackers

Two star trackers, used for attitude knowledge, are placed beside the FGM for high accuracy measurements. For this mission, the TERMA T1 star tracker has been chosen. The star trackers accuracy is $\leq$ 1.5 arcseconds cross boresight and 9 arcseconds cross roll sight. With an accuracy of 1.5 arcseconds the star tracker provides an accuracy of 0.24 nT, which is slightly above the scientific requirements. However, the performances still fulfill the mission requirements. The star trackers parameters are listed in the table below.

	m [g]	Size [mm]	P [W]	U [V]
Optical head	310	Ø92, 68 height	0.75	5
Electronic box	450	100× 100 × 40	2.5	28

Table 8: Star trackers parameters

3.4 Do we need a boom?

The boom is necessary to provide magnetic cleanliness to the instruments. In fact, the magnetic field provided by the satellite can affect the measurements, which have to be very precise to fulfill our science case. The length of the boom is estimated by $\frac{\Delta B}{V} = \frac{B_0}{d^3}$ with V = 10 cm×20 cm×30 cm. It leads to d = 1.1 m, if we consider that B_o=50 nT is the estimation of the full flux bus and ΔB <0.2 nT is the required accuracy.

3.5 GNSS

The FOTON GNSS receiver is chosen for our mission. The requirements are listed in Table 9. Following in Table 10, some performances of FOTON are listed. The provided lifetime of the FOTON is two years. By estimating the survival probability(n) for t = 3 years in Equation 1, it is calculated that there is a 74% chance for the FOTON to survive the duration of the mission time.

It is possible to replace the FOTON with a BLACKJACK which has a higher lifetime and performances in terms of total radiation dose.

$$e^{-\frac{\beta}{\alpha}\cdot t} = n \quad (1)$$

α = 10krad Si, β = 1krad/year.

Sampling	0.1 Hz
Accuracy	<30mm
Dual frequency	Yes

Table 9: Scientific requirements

Weight [g]	Size [mm]	Power [W]	Voltage [V]
350	83×96×38	4.8	3.3

Table 10: FOTON parameters

3.6 Payload cost estimation

The costs of the instruments are estimated as their prices are not available. The costs of the Fluxgate and the Scalar magnetometer are listed in Table 11.

	Person-power	Development time	Total cost
FGM	2-3	2y	500k€
CDSM	1-3	1y	250k€

Table 11: Cost for the FGM and ABS

The cost has been estimated considering 100 k€/y. The costs of the GNSS receiver and star trackers are listed in Table 12.

	Price	Cost estimated
GNSS	27k€	
STR		100k€

Table 12: Cost for the GNSS and STR

The cost for the star trackers is estimated on the basis of a similar instrument with lower performances. The total cost for the payload will be around 2.6 M€.

4 Mission

The mission analysis investigates the adequate orbits to fulfill scientific requirements as well as power generation, communication, and thermal needs.

4.1 Orbit selection

In order to achieve the scientific objectives an orbit configuration that enables 3D measurements of the Earth's magnetic field must be selected. A tetrahedral formation of 4 small satellites is proposed, with the required distances of 100-200 km between satellites. For the temporal and spatial resolution several requirements were identified as design drivers (see table below). The mission duration shall be 3 years, in order to measure long-term changes in the surveyed fields.

No.	Spatial	Temporal	Description
1	90 °	2h	LocalTime fixed; full B tensor for Lat.¡65°
2	22.5 °	12h	Earth fixed
3	72 °	12h	Earth fixed, for gravity

Table 13: Resolution requirements

4.1.1 Constellation Design

A tetrahedral formation of 4 satellites is achieved by the combination of 3 satellites on a so-called cartwheel orbit and a fourth satellite on a helix orbit ([Nogueira et al., 2015]). The selected orbit altitude of 400 km is based on a trade-off between the mission duration and the sensitivity of the instrument. To fulfill requirement no. 2, two constellations consisting of 4 satellites are needed, which fly on the same orbital plane with an offset in mean anomaly M of 180°. In addition, to fulfill requirement no. 1, two orbit planes differing by 90° in right ascension of the ascending node Ω are used. In order to reduce the costs of the design, integration, and testing of the satellites, all satellites should be identical and have the same solar panel configuration. For this purpose, the two orbit planes for sun-synchronous orbits are selected with a local time of ascending/descending node LTAN of 9AM and LTDN of 3PM.

In the table below the Keplerian elements for each satellite are listed.

Parameter	S1 / S5	S2 / S6	S3 / S7	S4 / S8
a [km]	6768	6768	6768	6768
e [-]	0.00453319	0.00453319	0.00453319	0.0001
i [deg]	97.0054	97.0054	97.0054	97.0054
Ω [deg]	Ω(1) / Ω(1)+90	Ω(1)+0.2 / Ω(5)+0.2	Ω(1)+0.1 / Ω(5)+0.1	Ω(1)1.4 / Ω(5)+1.4
ω [deg]	ω(1)	ω(1)+120	ω(1)+240	ω(1)-90
M [deg]	360-ω(1)	M(1)+240	M(1)+240	360-ω(1)

Table 14: Keplerian Orbit Elements

Requirements for the power and thermal control system are derived from the orbital period duration of 92 min and the eclipse duration of 36 min.

4.1.2 Collision risk and EOL consideration

Regarding the collision risk, the European Code of Conduct for Space Debris Mitigation indicates that the probability of collision with objects larger than 10 cm over the lifetime to be less than 0.001. This probability was calculated with the ARES DRAMA tool to be 2.3688e-05.

Regarding the EOL de-orbiting in LEO, after an operational lifetime of 3 years, the passivized spacecraft for the given orbit was calculated to have a decay time of around 1.4 years in the worst-case scenario.

4.2 Δv Budget

The Δv budget is driven by 2 main factors: the commissioning of each cartwheel helix formation and the compensation of perturbation acting on each of the spacecraft. As ESA margin philosophy for science assessment studies indicates, a margin of 20% on the calculated values and a 2% margin for EOL have to be taken into consideration for the total Δv budget.

	Delta v	Times	w/ margins
Commissioning	100 m/s	1	122.00m/s
Perturbations	11.4 m/s	18	250.35 m/s
		TOTAL	**372.35 m/s**

Table 15: Δv Budget

4.3 Launch

Two launchers are necessary since two orbital planes are considered. Table 4.3 lists all available commercial launchers. The SpaceX Falcon 9 is the cheapest one and is selected for this mission.

Rocket	k€/satellite	k€/constellation
Soyuz	195	780
Vega	250	1000
Falcon9	27	110
SpaceFlight (broker)	545	2180
Electron	480	1920
PSLV	315	1260

Table 16: Commercial launchers for CubeSats

5 Spacecraft design

5.1 Propulsion

The lifetime and formation flight requirements impose the need to use a propulsion system in each of the satellites comprising the mission.

5.1.1 Overview of technologies

There are several propulsion technologies that could be implemented on a CubeSat, as it can be seen on Table 17.

Type	Thrust	Isp [s]	Propellant mass
Cold Gas	10 mN – 10 N	40 - (70)	6.28 kg
Monopropellant	0.1 – 10 N	200 - (300)	1.78 kg
Arcjet	0.1N	500- (1500)	0.38 kg
FEEP	1 – 10 mN	(6000) - 10000	0.09 kg
PPT	1 – 1300 μN	650 - (1350)	0.42 kg

Table 17: Overview of available technologies

5.1.2 Propulsion system down-selection

For the final selection of the propulsion system several drivers are taken into account: TRL status, propellant type (ground handling), power consumption, specific impulse (required propellant mass) and available thrust.

After a market study of applicable propulsion systems for CubeSats and a subsequent trade-off study of the main drivers, the IFM Nano thruster from Enpulsion was selected. The thruster uses Field Emission Electric Propulsion technology (FEEP). The benefits of this technology are: very high specific impulses and efficiencies. The drawbacks of this technology are: low thrust capabilities and relatively high power consumption. The IFM Nano Thruster has been technologically demonstrated in space, which reduces the risk of the propulsion selection, specially for small satellites.

5.1.3 Propulsion operation

In the mission of study, when the propulsion system is operating, the science measurements have to be interrupted. There are two operation proposals: a conventional one and an innovative solution suited for electric propulsion.

In the conventional operation, the thrust manoeuvres for station keeping are performed when the semi-major axis

is lower than an imposed threshold (10Km). This requirement equates to a 2 month interval between thrust manoeuvres.

Due to the low thrust capabilities of the selected system each manoeuvre would require 3 days. Owing to the large time required per manoeuvre, a new operation philosophy is presented: more frequent manoeuvres but shorter in time.

	Conventional	**Proposed**
Manoeuvre frequency	60 days	3 orbits
Delta v	11.4 m/s	0.04 m/s
Manoeuvre time	76 h	10-15 min
Science interruption	Yes	No

Table 18: Conventional vs proposed operation

5.2 Thermal Control System

The Thermal Control System ensures no satellite component experiences a temperature outside of its operational limits. A Thermal Budget showed the batteries were the constraint, limiting the on-board temperature to the range 0°C to 40°C. The heat fluxes incident on the spacecraft are calculated as follows: solar flux Q_{solar} = $1371 W/m^2$, Earth albedo Q_{albedo} = $261 W/m^2$, Earth infra-red Q_{IR} = $210 W/m^2$. During eclipse the solar and albedo fluxes are zero. The internal heat generation is estimated to be 7.8 W (95% loss). By surface area the sun-pointing face consists of 70% solar cells (GaAs: emissivity $\epsilon = 0.85$, absorptivity $\alpha = 0.92$) and 30% high emissivity white painted aluminium ($\epsilon = 0.9$, $\alpha = 0.1$). All other faces of the spacecraft are coated in TEF Teflon to radiate heat into space ($\epsilon = 0.8$, $\alpha = 0.1$). With this construction the spacecraft reaches a maximum temperature of 20°C just before entering eclipse and falls to a minimum of – 8°C at the end of eclipse. This is not far below the lower limit of 0°C and more detailed thermal design will ensure the limit is not breached.

5.3 Attitude Determination and Control System (ADCS)

The external torques acting on the satellite are caused by atmospheric drag, solar radiation, the Earth's magnetic field, and the gravity gradient. At 400 km altitude drag has the largest effect (1.68x10-3 Nm), solar radiation torque is negligible, and the magnetic field is accounted for with the magnetic cleanliness programme. The solar arrays must point to the sun and the antenna and to the ground, with an accuracy of 5° and stability of 1°. A sun sensor on the solar array face (+Y) and earth sensor on the – Z face (Nadir facing) achieve these requirements. Two star trackers on the boom ensure give attitude knowledge to 1.5 arcseconds. An ADCS board with PID control sends commands to a 3-axis magnetorquer with a sufficient nominal actuation level of 0.2 Am^2 for attitude control (ISIS iMTQ). A reaction wheel constantly holds a magnetic field so is not included so as to not interfere with magnetometer measurements. For this reason an air core magnetorquer is used as it has no remnant magnetic field when unpowered. The ADCS modes are stand-by, safe, detumble (with B-dot control), pointing, and orbit control.

5.4 Telecommunication and link budget

5.4.1 Requirements

The data requirements for the different instruments of the payload and house keeping are summarized in the table below.

Requirements	Daily data
GPS data	80 Mbits
Flux gate magnetometer	5 Mbits
Coupled dark state magnetometer	0.4 Mbits
2 star trackers	11 Mbits
House keeping data	10 kbits

Table 19: Amount of daily data to send to the ground station

A total of 390 Mbits must be transmitted to Earth every day for each formation of four satellites. The amounts of data needed are computed from the range, the resolution and the acquisition frequency of each instrument.

5.4.2 Space segment

To reach this objective data rate, S-band frequency was selected. This frequency band has on one hand the advantage of providing higher data rates than VHF and UHF frequency (usually limited to a couple of 100 kbps) and on the other hand it does not need precise pointing mechanism required for higher band frequencies such as X-band. To release the constraints on ground operations, just one satellite downlinks measurements so the antenna ground station needs to track only one satellite. Data needs to be transmitted each day during a visibility window of 5 minutes. The existence of this daily 5 minute visibility window was confirmed by STK simulations. This satellite, called the master, receives the data measurements from the three other satellites, the so-called slaves, during 50 minutes transmission per day. Inter-satellite links are then needed,they are ensured by the same S-band antenna as for the communication with the ground.

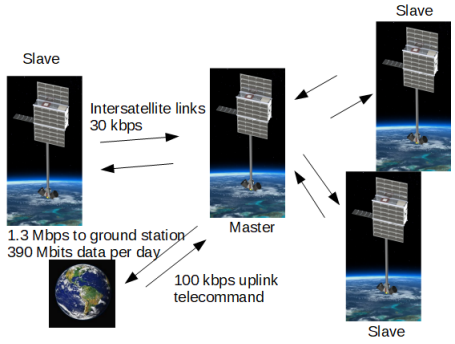

Figure 3: Master slave architecture with intersatellite link

A simple approach to ensure the link between satellites is to position a second S-band antenna on the opposite side of the satellites. This way, the two S-band antennas cover two half hemispheres and enable a complete coverage without attitude control. A switch is required to select the antenna with the best signal over noise ratio. The fact that the satellites use the same antennas, receiver and transceiver for inter-satellite links and links with the

ground station permits a seamless substitution of the master satellite by a slave in case of failure without including extra hardware in the satellite bus. Link budget calculations showed that the required signal over noise ratio could be met with 1W RF power provided by the S-band transmitter.

5.4.3 Ground segment

The ground station is positioned in Kiruna (Sweden) and is owned by ESA. The large 15m S-band antenna alleviates the power and antenna requirements on satellites. The characteristics of the ground stations are presented in the following table.

Ground station characteristics	Value
Latitude/Longitude	67°/20°
Diameter antenna	15 m
EIRP	101 dBm
G/T	27 dB/K
Angular speed	5°/s

Table 20: Ground station characteristics

The antenna from the ground station is fast enough to track the satellites at 400 km which have 4.2°/s angular speed on their orbit.

5.5 On-Board Computer (OBC)

5.5.1 ISIS OBC

The COTS On-Board Computer from ISIS with a 400MHz 32-bit ARM9 processor is recommended for CubeSats and is assessed status 9 in the TRL scale. It provides common interfaces like I2C, SPI, CAN and GPIO, and an ADC 8 channel/10-bit. Data up to 32GB can be stored. The properties show a power consumption of around 400mW, dimensions of 96 × 90 × 12.4mm and a mass of 100 g (ISIS).

5.5.2 Housekeeping

To verify the health of modules in a satellite a housekeeper module is implemented. Due to a periodic checkup, the current state of the satellite can be analysed and in given cases, the faulty module will be reset to prevent greater damage. Phases include error detection, damage confinement and assessment, error recovery, and fault treatment and continued service. A satellite network check will be done before the module check, which comes along with basic catch-all measures. ([Normann, 2016])

5.6 Power modes

To estimate the power management the power consumption and the power generation were estimated. Based on calculations it is not needed to have a power controller. The end of life is taken into account in the margins.

5.6.1 Science mode

First, the power budget was done using peak power consumption P_{peak} of all subsystems needed and gathered into a table. To better estimate the duty cycle of each subsystem a power budget of a past mission as be taken as an example. To do so, a difference was made between power needed during eclipse P_e and the daylight time power P_d.

Subsystem	P_{peak} (W)	P_e (W)	P_d (W)
ADCS	1.3	0.81	0.85
Telecom	7.4	0.5	0.5
Payload	9.2	5.84	5.84
Propulsion	20	3.5	3.5
Deployment	1.5	0	0
Total (+20%)		**12.78**	**12.83**

Table 21: Power budget

5.6.2 Solar panel sizing

According to the power budget below, the system needs a power of 12.78W during eclipse and 12.83W during daylight time. According to the inclination of solar panel, the 45 deg angle has to be taken into account. In order to determine the area of solar panel needed to produce this power, the following formula was used :

$$P_{sat} = \frac{\frac{P_e.T_e}{X_e} + \frac{P_d.T_d}{X_d}}{T_d} = 39W \quad (2)$$

T_e and T_d are respectively the duration of the eclipse and the daylight time. X_e and X_d represent the efficiency of the paths from solar array through the batteries to individual loads. The direct energy transfer is used, so $X_e = 0.65$ and $X_d = 0.85$.

Silicon solar cell are chosen because it is a good compromise between efficiency ($\eta = 22\%$) and price. To produce the power needed, it is required to have a solar panel area of at least $0.13m^2$. Furthermore, a degradation of 3.75% a year and 20% margin are to be taken. So final area needed is :

$$A_{SP} = 0.17m^2 \quad (3)$$

5.6.3 Launch and Early Operations Phase (LEOP) and Commissioning

The battery has to be chosen according to the eclipse time. The battery also have to be big enough to supply the spacecraft during Launch and Early Orbit Phase.

Subsystem	P_{peak} (W)	P_{LEOP} (W)
ADCS	1.3	1.3
Telecom	7.4	2.5
Propulsion	20	13.5
Deployment	1.5	1.5
Total (+20%)		**22.56**

Table 22: LEOP power budget

The LEOP is considered as during 2 hours at P_{LEOP} in order to have the energy needed, the launch and initialisation time T_l usually last 3 days.

5.6.4 Battery and Electrical Power System (EPS)

Calculations are based on a depth discharge DOD of 20%, on a transmission efficiency of 0.9 and a margin of 20% is taken. It gives the energy needed E_n of 51 Wh. The EPS is chosen depending on this calculation, it provides 22.5 Wh, so two VES16 batteries are added to it in order to reach E_b 54.5 Wh. Based on this number it is possible to determine the time T_{dep} (in hours) after launch the solar panels are to be deployed.

$$T_{dep} = \frac{DOD.E_b.T_l}{E_n} = 15h \tag{4}$$

So, solar panel have to be deployed 15 hours after launch in order to reach the power budget.

6 Risk and cost

6.1 Risk

Space missions are complex and expensive projects that require the use of risk management to guarantee success.

In risk analysis, a distinction is made between the probability of occurrence and the degree of severity in order to classify the individual failure cases and to elaborate solutions for the very high-risk areas.

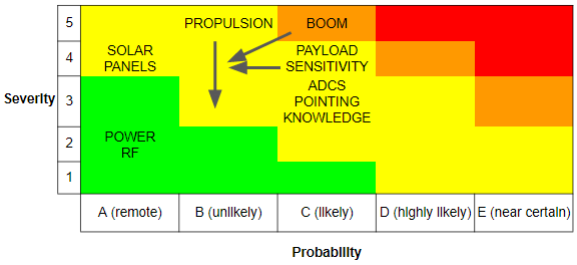

Figure 4: Risk Assessment Matrix

The propulsion, ADCS and payload were identified as medium-risk subsystems of the RUBIKS mission. In order to continue the mission in case of a failure of the propulsion of a satellite, an additional spare satellite can fly parallel to the formation. On the other hand, to reduce the probability of a failure of the instrument sensitivity or the deployment mechanism of the boom, additional tests can be performed to verify their reliability.

Finally, ADCS knowledge integrity can also be improved if more expensive star sensors are used.

6.2 Cost

To compute the total cost of the mission, it is divided into two parts: CubeSat/Satellite and the operational phase.

The price for a satellite bus is 450 k€ and the total development is estimated to 2 years with 3 person-year (100 k€/pers), which lead to 4.6 M€ for the 8 satellite buses.

Each satellite needs to be assembled, integrated, verified and tested (AIV/AIT). Especially magnetic cleanliness needs to be characterized and mitigated (50 nT assumed acceptable value). It leads to a cost of 500 k€ for the 2 constellations.

The payload cost, as explained in section 3.6, is 2.6 M€. The Falcon 9 is chosen, as presented in section 4.3, is 220 k€:

The whole platform cost is therefore 7.92M€.

For the operational cost, the ground segment as well as the data analysis is considered. A operational lifetime is considered with only one operator during this time thanks to automation and 3 scientists. It leads to 1.2 M€.

The overall cost of the mission is around 9 M€ and with a 20% margin, 10.7 M€.

To reduce risks a solution as discussed in the previous section is to add a **spare satellite** into each constellation. The operational cost stays the same while the CubeSat part is **increased by 1.5 M€**. It leads to a total cost of 10.5 M€ and 12.5 M€ with 20 % margin.

7 De-scoping options

There is no option to reduce the number of satellites below 8 to achieve the stated science requirements. Only one flight of 4 satellites can not resolved the spatial observations requirements to build the model.

Removing gravity gradient measurements is not an option because the hardware is already required for the propulsion system.

8 Conclusion

RUBIKS is a mission which combined magnetic and gravity mission to resolve the composition and dynamics of the mantle, and offer a better constrain on the outer core dynamics. It is a low cost 3 years mission (10 M€), with a 2 years development time, employing interconnected CubeSats on formation flying. The formation offers several free science applications like GNSS TEC, ionospheric studies, neutral winds, and density estimations for the upper Atmosphere.

References

[Deschamps and Khan, 2016] Deschamps, F. and Khan, A. (2016). Electrical conductivity as a constraint on lower mantle thermo-chemical structure. *Earth and Planetary Science Letters*, 450:108–119.

[Dewey and Burke, 1973] Dewey, J. F. and Burke, K. C. A. (1973). Tibetan, Variscan, and Precambrian Basement Reactivation: Products of Continental Collision. *The Journal of Geology*, 81(6):683–692.

[Dutta and Mandal, 2017] Dutta, U. and Mandal, N. (2017). Pulsating dynamics of thermal plumes and its implications for multiple eruption events in the Deccan Traps, India. *arXiv:1703.00085 [physics]*. arXiv: 1703.00085.

[Garnero et al., 2016] Garnero, E. J., McNamara, A. K., and Shim, S.-H. (2016). Continent-sized anomalous zones with low seismic velocity at the base of Earth's mantle. *Nature Geosci*, 9(7):481–489.

[Gassmöller et al., 2016] Gassmöller, R., Dannberg, J., Bredow, E., Steinberger, B., and Torsvik, T. H. (2016). Major influence of plume-ridge interaction, lithosphere thickness variations, and global mantle flow on hotspot volcanism-The example of Tristan: PLUME-RIDGE INTERACTION OF TRISTAN. *Geochem. Geophys. Geosyst.*, 17(4):1454–1479.

[Harrison et al., 2017] Harrison, L. N., Weis, D., and Garcia, M. O. (2017). The link between Hawaiian mantle plume composition, magmatic flux, and deep mantle geodynamics. *Earth and Planetary Science Letters*, 463:298–309.

[Jäggi et al., 2011] Jäggi, A., Bock, H., Prange, L., Meyer, U., and Beutler, G. (2011). GPS-only gravity field recovery with GOCE, CHAMP, and GRACE. *Advances in Space Research*, 47(6):1020–1028.

[Jäggi et al., 2016] Jäggi, A., Dahle, C., Arnold, D., Bock, H., Meyer, U., Beutler, G., and van den IJssel, J. (2016). Swarm kinematic orbits and gravity fields from 18 months of GPS data. *Advances in Space Research*, 57(1):218–233.

[Khan et al., 2007] Khan, A., Connolly, J. A. D., Maclennan, J., and Mosegaard, K. (2007). Joint inversion of seismic and gravity data for lunar composition and thermal state. *Geophysical Journal International*, 168(1):243–258.

[Koelemeijer et al., 2016] Koelemeijer, P., Ritsema, J., Deuss, A., and van Heijst, H.-J. (2016). SP12RTS: a degree-12 model of shear- and compressional-wave velocity for Earth's mantle. *Geophys. J. Int.*, 204(2):1024–1039.

[Koptev et al., 2018] Koptev, A., Burov, E., Gerya, T., Le Pourhiet, L., Leroy, S., Calais, E., and Jolivet, L. (2018). Plume-induced continental rifting and break-up in ultra-slow extension context: Insights from 3D numerical modeling. *Tectonophysics*, 746:121–137.

[Mandea et al., 2012] Mandea, M., Panet, I., Lesur, V., de Viron, O., Diament, M., and Le Mouel, J.-L. (2012). Recent changes of the Earth's core derived from satellite observations of magnetic and gravity fields. *Proceedings of the National Academy of Sciences*, 109(47):19129–19133.

[Miao et al., 2019] Miao, X.-Q., Zhang, X., Zhang, H., Wang, J.-R., Liu, Z., Li, C.-Z., Shi, Q., Li, R.-W., Huang, Y.-S., and Ma, Q.-Z. (2019). Geochronological and geochemical studies of the OIB-type Baiyanghe dolerites: implications for the existence of a mantle plume in northern West Junggar (NW China). *Geol. Mag.*, 156(4):702–724.

[Murakami, 2004] Murakami, M. (2004). Post-Perovskite Phase Transition in MgSiO3. *Science*, 304(5672):855–858.

[Nogueira et al., 2015] Nogueira, T., Scharnagl, J., Kotsiaros, S., and Schilling, K. (2015). NetSat-4G A four nano-satellite formation for global geomagnetic gradiometry. page 9.

[Normann, 2016] Normann, M. A. (2016). Software Design of an Onboard Computer for a Nanosatellite. page 121.

[Püthe et al., 2015] Püthe, C., Kuvshinov, A., and Olsen, N. (2015). Handling complex source structures in global EM induction studies: from C-responses to new arrays of transfer functions. *Geophysical Journal International*, 201(1):318–328.

[Rawlinson et al., 2014] Rawlinson, N., Fichtner, A., Sambridge, M., and Young, M. K. (2014). Seismic Tomography and the Assessment of Uncertainty. In *Advances in Geophysics*, volume 55, pages 1–76. Elsevier.

[Sabaka and Olsen, 2006] Sabaka, T. J. and Olsen, N. (2006). Enhancing comprehensive inversions using the Swarm constellation. *Earth Planet Sp*, 58(4):371–395.

[Sleep, 2006] Sleep, N. H. (2006). Mantle plumes from top to bottom. *Earth-Science Reviews*, 77(4):231–271.

[Trampert, 2004] Trampert, J. (2004). Probabilistic Tomography Maps Chemical Heterogeneities Throughout the Lower Mantle. *Science*, 306(5697):853–856.

[van Keken et al., 2002] van Keken, P. E., Hauri, E. H., and Ballentine, C. J. (2002). Mantle Mixing: The Generation, Preservation, and Destruction of Chemical Heterogeneity. *Annu. Rev. Earth Planet. Sci.*, 30(1):493–525.